Supplement of Atmos. Chem. Phys., 25, 7959–7972, 2025
https://doi.org/10.5194/acp-25-7959-2025-supplement

Atmospheric Chemistry and Physics
Open Access

Supplement of

Source-dependent optical properties and molecular characteristics of atmospheric brown carbon

Jinghao Zhai et al.

Correspondence to: Xin Yang (yangx@sustech.edu.cn)

Text S1. Online instrument descriptions. During the field campaign, an aethalometer (AE31, Magee Scientific, USA) measuring at seven wavelengths (370, 470, 520, 590, 660, 880, and 950 nm) and a photoacoustic extinctiometer (PAX, Droplet Measurement Techniques, USA) measuring at 532 nm, were utilized to detect the online optical properties of particles. The absorption coefficient (b_{abs}) derived from the aethalometer is calculated as follows:

$$b_{\mathrm{abs}}(\lambda) = \mathrm{MAC}_{\mathrm{AET}}\, C_{\mathrm{BC,AET}}$$

where λ is the wavelength, $\mathrm{MAC}_{\mathrm{AET}}$ = 14625/λ (m^2/g) is the manufacturer's specified mass absorption cross-section, and $C_{\mathrm{BC,AET}}$ is the BC concentration reported by the instrument. The aethalometer results were corrected for both the absorption enhancement due to multiple scattering in the collection filter and the decrease in the aethalometer response with increasing particle loading (Weingartner et al., 2003;Arnott et al., 2005).

Previous studies have reported that the b_{abs} estimated from the aethalometer is generally larger than that measured by the PAX, likely due to artifacts associated with organic matter loading on the filter (Lack et al., 2008;Cappa et al., 2008;Saleh et al., 2014). The correlation between the b_{abs} obtained from the aethalometer ($b_{\mathrm{abs,520}}$) and the PAX ($b_{\mathrm{abs,532}}$) is shown in Figure S2. In this study, the aethalometer-derived b_{abs} were scaled by a factor of 2 for all wavelengths.

Text S2. Pretreatment of the sample filters. The sample filters were punched into 1 cm^2 pieces for extraction. Each sample was ultrasonically extracted in deionized water at room temperature. The extract was filtered through a 0.22 μm glass fiber filter. The original extract was used directly for absorbance measurements. To achieve adequate analyte concentrations of mass spectrometry, the extraction process was repeated three times (Zhang et al., 2023). Then, the extract was freeze-dried and concentrated to 0.5 ml for further analysis.

Text S3. Operating principle of the OC/EC analyzer. The OC/EC analyzer functions by selectively oxidizing OC and EC at specific temperatures and in different atmospheric conditions. Organic compounds are volatilized from the sample deposit in an inert helium environment, while EC requires combustion in the oxidizing atmosphere. The process involves:

(1) extracting carbon compounds at various temperatures and oxidation settings from a ~0.5 cm^2 punch of quartz-fiber filter; (2) converting these compounds to carbon dioxide (CO_2) using a heated manganese dioxide (MnO_2) oxidizer; and (3) quantifying CO_2 with a nondispersive infrared (NDIR) CO_2 detector.

The analyzer measures seven specific temperature fractions (OC1-4, up to 580°C, and EC1-3, up to 840°C) that can be individually reported. Key reported values include total OC, total EC, total carbon (TC, the sum of OC and EC), and pyrolyzed carbon, monitored by both optical reflectance (OPR) and transmittance (OPT). Depending on the thermal and optical protocol used, thermally-derived OC and EC subfractions, as well as carbonate carbon, are also quantified.

Text S4. Calculation of the molecular absorption contribution. A partial least squares regression (PLSR) model was used to calculate the molecular absorption contribution detected by the photodiode array (PDA). Suppose the brown carbon system is a dilute solution, where each substance satisfies the Lambert-Beer law. That is, the absorption of each component $b_{\mathrm{abs,i}}$ is proportional to the product of its molar absorption coefficient ϵ_{i} and concentration c_{i}, and the total absorption is the sum of the absorptions of all components, given by:

$$b_{\mathrm{abs,370}} = \sum b_{\mathrm{abs,i,370}} = \sum \epsilon_{\mathrm{i}}\, c_{\mathrm{i}} = \sum \beta_{\mathrm{i}}\, I_{\mathrm{max,i}}$$

Here, β_{i} is the absorption contribution coefficient of the brown carbon molecule and obtained through the PLSR fitting, and $I_{\mathrm{max,i}}$ is the mass spectrometric response signal of the brown carbon molecule. In this study, the programming code for PLSR was implemented using the scikit-learn (v 1.2.0) package in Python (Pedregosa et al., 2011).

The identification of molecular structures was performed by Sirius (v 5.83). Sirius operates by integrating isotope information from MS1 spectra and fragment ion information from MS2 spectra, and searching molecular structures via online databases. The absorbance spectra of the identified BrC molecules were simulated using Gaussian. Molecular geometries were optimized at the B3LYP/6-311G** level to determine the most stable conformations. Subsequently, UV-Vis absorption spectra were simulated for these optimized structures using

the PBE1PBE/TZVP model, with water as the solvent modeled by the IEFPCM method.

Molecular models were optimized and their ultraviolet-visible (UV-Vis) absorption energies were calculated using Gaussian. The resulting data were subsequently visualized with Multiwfn (v 3.8). A total of 501 theoretical single-molecule absorbance values were computed for 169 molecules. For each molecule, up to three conformers were considered, and the conformer exhibiting the highest molar absorptivity at 370 nm was selected to estimate the optical contribution. Given that the optical contribution is jointly influenced by both molar absorptivity and molecular concentration, and that the concentration of each component could not be determined in this study, a molar absorptivity threshold of 1000 was adopted to identify structures with significant absorption. Among the 169 molecules, 24 satisfied this criterion. The structural information for these molecules is summarized in Table S1.

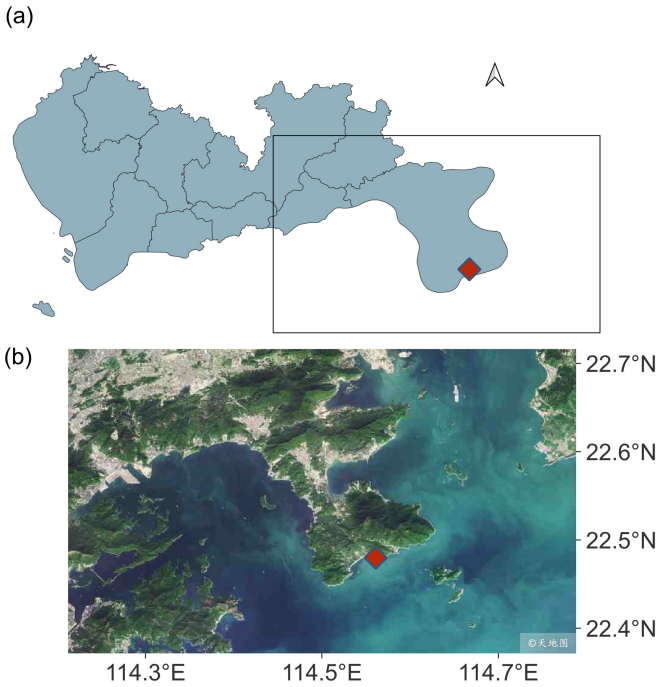

Figure S1. Maps of the sampling site. (a) Administrative areas of Shenzhen city. (b) Satellite image of the framed area in (a). The asterisk represents the sampling site of Xichong (22.48ºN, 114.56ºE). The maps were created with QGIS (v 3.16). The satellite image is from www.tianditu.gov.cn.

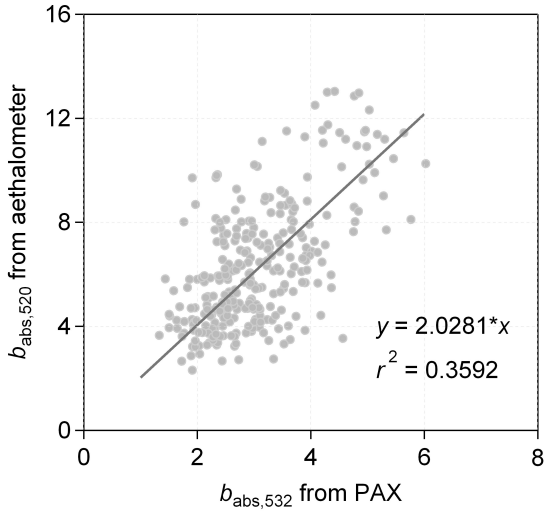

Figure S2. The correlation of absorption coefficients (Mm^{-1}) derived from the aethalometer ($b_{\mathrm{abs,520}}$) and the PAX ($b_{\mathrm{abs,532}}$).

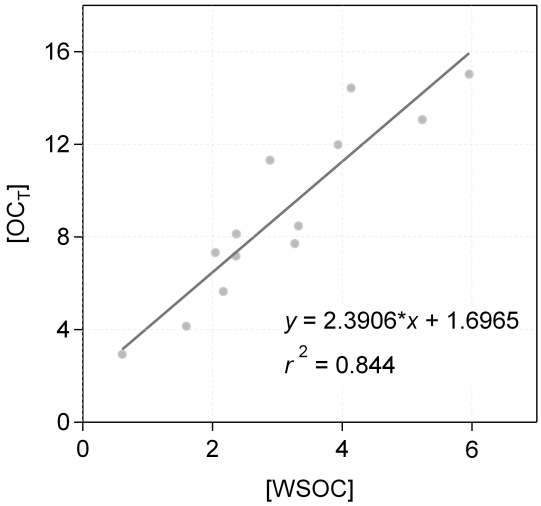

Figure S3. The correlation of BrC mass concentration (μg/m^3) detected by the thermal desorption method ([OC_T]) and the dissolution method ([WSOC]).

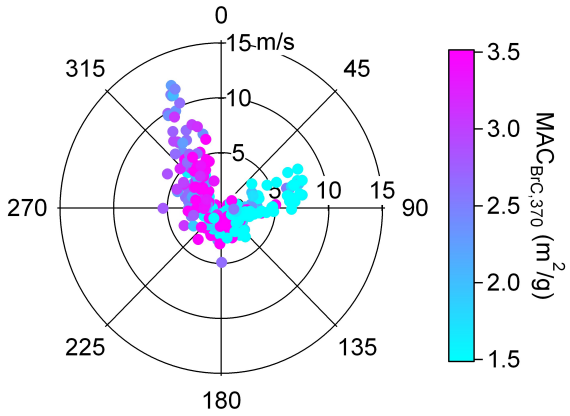

Figure S4. Polar plot and $MAC_{BrC,370}$ values from online measurements. The radius and color represent the values of $MAC_{BrC,370}$ in the downwind direction at specific wind speeds. The color scale denotes the values of $MAC_{BrC,370}$.

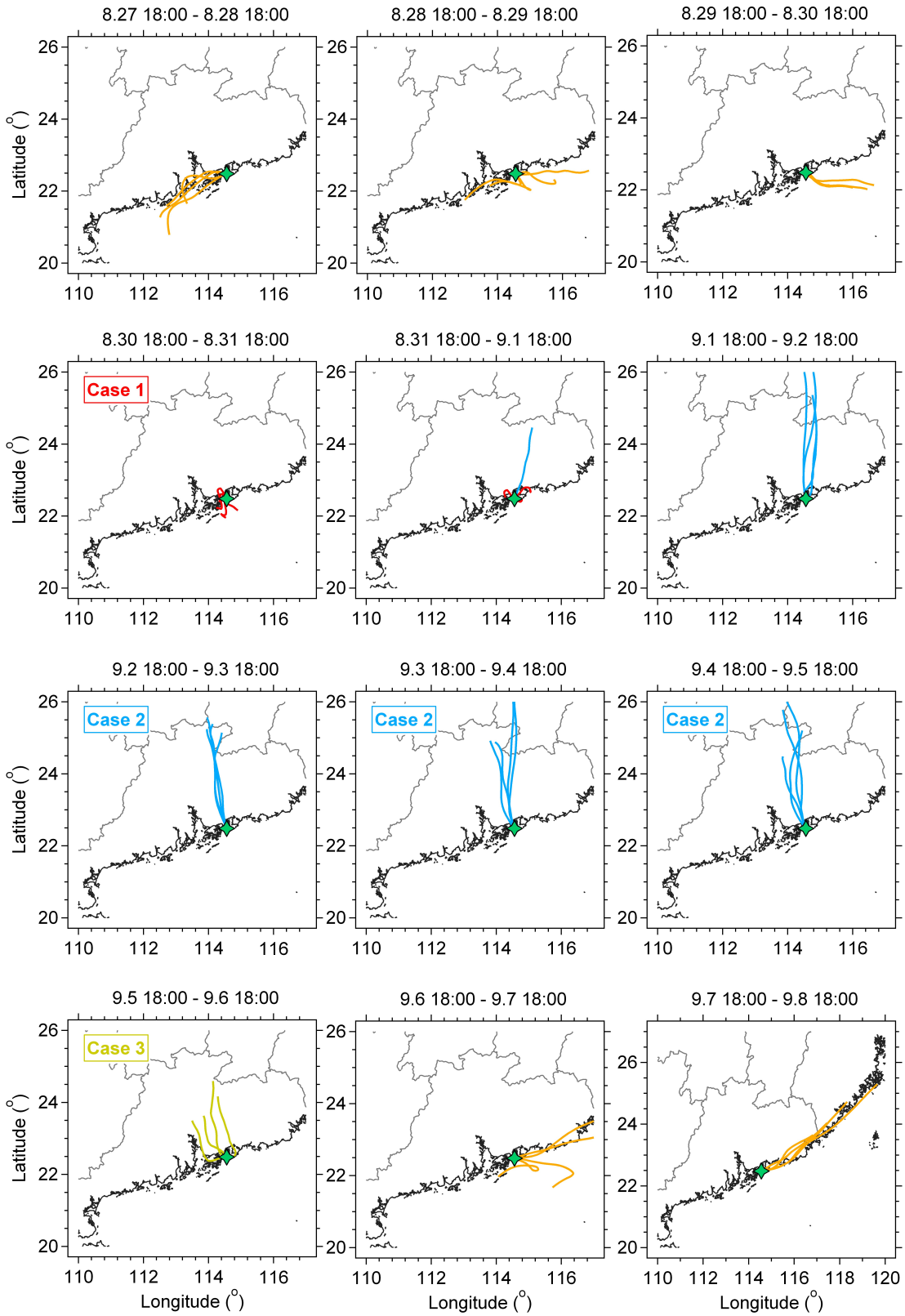

Figure S5. The HYSPLIT 24-hour air mass backward trajectories at a 50 m arrival height, ending at 0:00, 6:00, 12:00, and 18:00 (UTC+8) each day during the sampling period from 8/27/2022 to 9/8/2022.

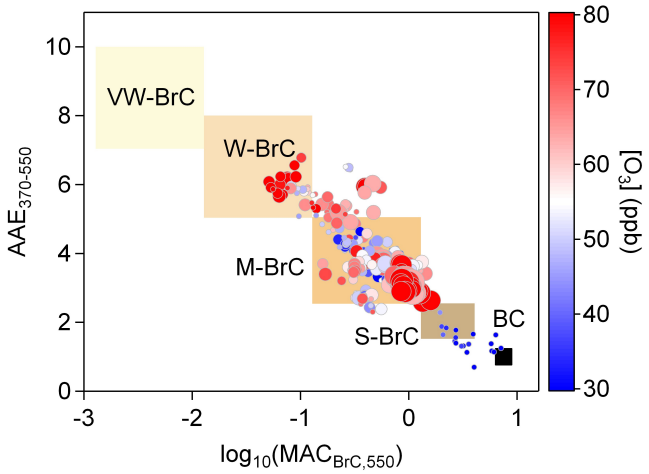

Figure S6. Optical-based BrC classification scheme (Saleh, 2020) in the log10 ($MAC_{BrC,550}$ [m^2/g]) vs. $AAE_{370-550}$ space for online measurements throughout the whole sampling period. BrC mass concentrations used for the $MAC_{BrC,550}$ were determined based on thermally desorbed organic carbon. The color scale denotes the concentration of ozone in ppb. The size of scatters denotes the concentration of K^+ detected by the MARGA.

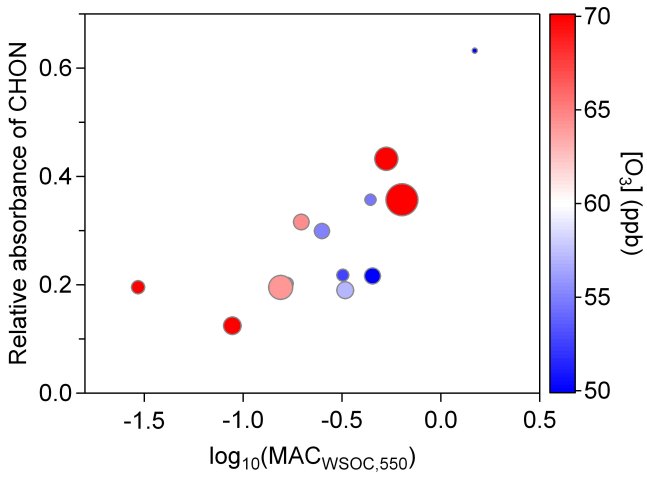

Figure S7. Relative absorbance of CHON detected in WSOC vs. log10 ($MAC_{WSOC,550}$ [m^2/g]) from offline filter-based measurements throughout the whole sampling period. BrC mass concentrations used for the $MAC_{WSOC,550}$ were determined based on water-soluble organic carbon. The color scale denotes the concentration of ozone in ppb. The size of scatters denotes the concentration of K^+ detected by the MARGA.

Table S1. Molecular formula, molecular mass (Da), simulated molar absorptivity ($L \cdot mol^{-1} \cdot cm^{-1}$) at 370 nm, and proposed structures of major light-absorbing BrC chromophores identified in this study.

Formula	Mass	Molar absorptivity	Structure
$C_{10}H_{10}O_4$	194.0579	69293.17	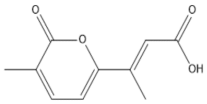
$C_{11}H_{10}O_6$	238.0477	45295.80	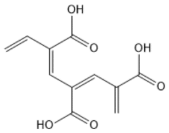
$C_{12}H_{11}N_3O_4$	261.0750	26961.74	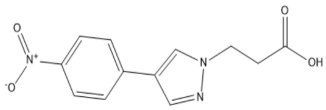
$C_{16}H_{18}O_9$	354.0951	15911.24	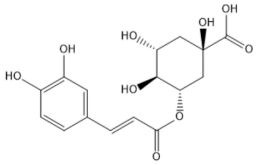
$C_{16}H_{14}N_4O_5S$	374.0685	13271.89	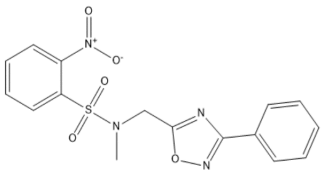
$C_9H_8O_5$	196.0372	11023.49	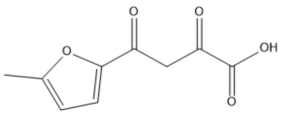
$C_7H_4N_2O_3$	164.0222	10251.14	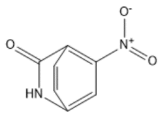
$C_8H_9NO_4$	183.0532	8124.25	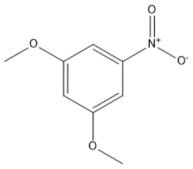
$C_6H_5NO_4$	155.0219	7677.53	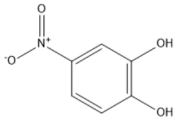
$C_6H_3N_3O_7$	228.9971	7596.25	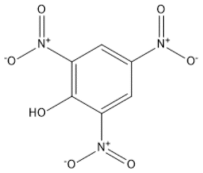

$C_7H_7NO_4$	169.0375	7418.68	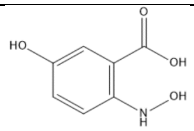
$C_{17}H_{20}O_8$	352.1158	6851.41	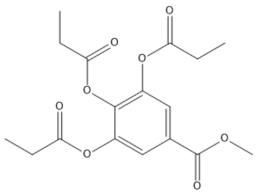
$C_7H_7NO_3$	153.0426	5679.85	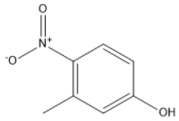
$C_8H_7NO_4$	181.0375	5214.56	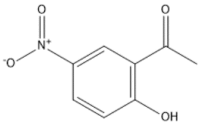
$C_7H_4N_2O_7$	228.0019	4790.78	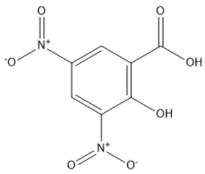
$C_7H_6N_2O_6$	214.0226	4587.31	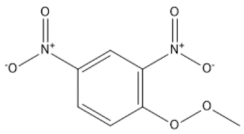
$C_7H_5NO_5$	183.0168	3414.05	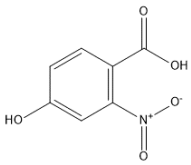
$C_7H_{10}N_6O_2$	210.0865	3385.22	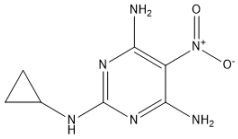
$C_6H_3N_3O_7$	228.9971	3252.82	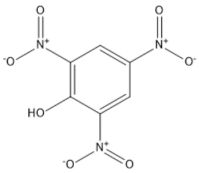
$C_6H_5NO_3$	139.0269	3219.28	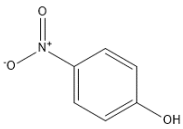

$C_6H_4N_2O_5$	184.0120	2604.79	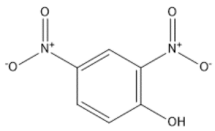
$C_9H_{10}O$	134.0732	2466.48	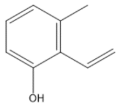
$C_{16}H_{22}O_2$	246.1620	1332.55	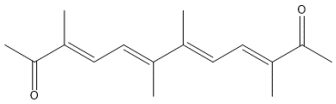
$C_{18}H_{17}N_7O_5S$	443.1012	1019.21	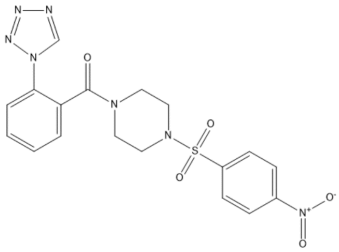

References:

Arnott, W. P., Hamasha, K., Moosmuller, H., Sheridan, P. J., and Ogren, J. A.: Towards aerosol light-absorption measurements with a 7-wavelength Aethalometer: Evaluation with a photoacoustic instrument and 3-wavelength nephelometer, Aerosol Sci. Technol., 39, 17-29, 10.1080/027868290901972, 2005.

Cappa, C. D., Lack, D. A., Burkholder, J. B., and Ravishankara, A. R.: Bias in filter-based aerosol light absorption measurements due to organic aerosol loading: Evidence from laboratory measurements, Aerosol Sci. Technol., 42, 1022-1032, 10.1080/02786820802389285, 2008.

Lack, D. A., Cappa, C. D., Covert, D. S., Baynard, T., Massoli, P., Sierau, B., Bates, T. S., Quinn, P. K., Lovejoy, E. R., and Ravishankara, A. R.: Bias in filter-based aerosol light absorption measurements due to organic aerosol loading: Evidence from ambient measurements, Aerosol Sci. Technol., 42, 1033-1041, 10.1080/02786820802389277, 2008.

Pedregosa, F., Varoquaux, G., Gramfort, A., Michel, V., Thirion, B., Grisel, O., Blondel, M., Prettenhofer, P., Weiss, R., Dubourg, V., Vanderplas, J., Passos, A., Cournapeau, D., Brucher, M., Perrot, M., and Duchesnay, E.: Scikit-learn: Machine learning in Python, J. Mach. Learn. Res., 12, 2825-2830, 2011.

Saleh, R., Robinson, E. S., Tkacik, D. S., Ahern, A. T., Liu, S., Aiken, A. C., Sullivan, R. C., Presto, A. A., Dubey, M. K., Yokelson, R. J., Donahue, N. M., and Robinson, A. L.: Brownness of organics in aerosols from biomass burning linked to their black carbon content, Nat. Geosci., 7, 647-650, 10.1038/ngeo2220, 2014.

Saleh, R.: From measurements to models: Toward accurate representation of brown carbon in climate calculations, Curr. Pollut. Rep., 6, 90-104, 10.1007/s40726-020-00139-3, 2020.

Weingartner, E., Saathoff, H., Schnaiter, M., Streit, N., Bitnar, B., and Baltensperger, U.: Absorption of light by soot particles: determination of the absorption coefficient by means of aethalometers, J. Aerosol Sci., 34, 1445-1463, 10.1016/s0021-8502(03)00359-8, 2003.

Zhang, A. T., Zeng, Y. L., Yang, X., Zhai, J. H., Wang, Y. X., Xing, C. B., Cai, B. H., Shi, S., Zhang, Y. J., Shen, Z. X., Fu, T. M., Zhu, L., Shen, H. Z., Ye, J. H., and Wang, C.: Organic matrix effect on the molecular light absorption of brown carbon, Geophys. Res. Lett., 50, 10.1029/2023gl106541, 2023.